

Temperature dependent growth of cadmium(II) oxide nanocrystals: studies on morphology based optical, electrical and dielectric properties

Shyamapada Shit¹ · Animesh Layek²

Received: 20 August 2015 / Accepted: 30 November 2015 / Published online: 14 December 2015
© Springer Science+Business Media New York 2015

Abstract Nanocrystalline cadmium(II) oxide were obtained by calcining a hydrated cadmium-organic hybrid precursor, $(C_{10}H_2O_8)Cd_2 \cdot xH_2O$, obtained by a chemical reduction method using cadmium acetate dihydrate, 1,2,4,5-benzenetetracarboxylic acid, and triethylamine. Calcined CdO at different temperature possess different morphology, revealed by field emission scanning electron microscope analysis. In this article, the photosensitivity, dielectric behavior, frequency dependant loss-tangent and complex impedance spectra of the morphology driven CdO nanoparticles were studied aptly.

1 Introduction

Nanocrystalline materials have paid special attention in the recent years for their inimitable and remarkable physical and chemical properties in comparison to their bulk properties or single atom [1, 2]. Nanocrystalline cadmium oxide (CdO) is a well-known n-type semiconductor metal oxide having a rock-salt crystal structure (FCC) with direct and indirect band gap within the range of 2.2–2.7 and 1.36–1.98 eV [3, 4], respectively. However, variations in the magnitude of these band gaps were reported in the literature due to the variations of the experimental conditions [5]. Nano-dimensional CdO bearing different morphologies such as nanoparticles, nanowires [6],

nanoneedles, nanotubes [7], nanorods [8] etc. were reported in the literature. Due to its high band gap and large linear refractive index ($n_o = 2.49$) it finds wide range of applications in solar cells, gas sensors, transparent electrodes and photodiodes, photocatalysts, optoelectronic devices [9–12], chemical sensors and liquid crystal display [13, 14], and many more. Numbers of methods including sonochemical, micro-emulsion, hydrothermal/solvothermal methods and mechanochemical processes [15–21] have been employed to get such fascinating CdO nano-structures. However, controlled growth of spherical CdO nanoparticles is still a challenging task. There are few reports on growing spherical CdO in the literature. Solvothermal method [4, 22] is cost effective and usually used in growing CdO nanoparticles. Sonochemical method using cadmium-organic precursors was also explored for growing spherical CdO nanoparticles [23, 24]. However, wet chemical reduction of cadmium-organic precursor for growing CdO nanoparticles was not well-explored [25–27]. Herein, we have successfully employed a chemical reduction method [28] of growing nano-crystalline CdO for the first time, using cadmium(II)-1,2,4,5-benzenetetracarboxylate hydrate precursor $[(C_{10}H_2O_8)Cd_2 \cdot xH_2O]$, obtained by the reaction of cadmium acetate dihydrate, 1,2,4,5-benzenetetracarboxylic acid, and triethylamine. The method is very simple, cost effective and does not require any special apparatus or techniques usually adopted in other methods of the synthesis of CdO nanoparticles. This method explores triethylamine $((C_2H_5)_3N)$, an unconventional base instead of conventional hydroxide bases. The base is mild compared to hydroxide and generates hydroxide ions through hydrolysis in water. Thus modulate the concentration of OH^- in the medium and avoid the precipitation of $Cd(OH)_2$. Its volatility also suggests that a little bit excess will not affect the overall

✉ Animesh Layek
layekanimesh@gmail.com

¹ Department of Chemistry, Jalpaiguri Government Engineering College, Jalpaiguri 735102, West Bengal, India

² Department of Physics, Bejoy Narayan Mahavidyalaya, Itachuna, Hooghly 712147, West Bengal, India

process though in our synthesis we have used stoichiometric amount of it.

In this article, the effect of temperature on the growth of the CdO nano-particles was studied. Mostly the effect of morphology on the optical, electrical and optoelectronic behaviour of the synthesized materials was investigated and demonstrated. The morphology driven dielectric property of the materials was analyzed by impedance spectroscopy technique.

2 Materials and methods

Cadmium (II) acetate dihydrate, triethylamine were purchased from E. Merck, India. 1,2,4,5-Benzenetetracarboxylic acid was purchased from Sigma Aldrich Co. Ltd. All chemicals were used as received.

Preparation of cadmium(II)-1,2,4,5-benzenetetracarboxylate hydrate precursor $[(C_{10}H_2O_8)Cd_2 \cdot xH_2O]$ and CdO nanoparticles therein: Cadmium(II) acetate dihydrate (40 mM, 10.661 g) was dissolved with constant stirring in 100 mL of distilled water taken in a 250 mL beaker. In another 100 mL beaker, 5.083 g of 1,2,4,5-benzenetetracarboxylic acid (20 mM) in 50 mL distilled water was dissolved by dropwise addition of triethylamine (80 mM, 8.09 g) with constant stirring. The solution containing triethylammonium 1,2,4,5-benzenetetracarboxylate was slowly added to the solution of cadmium(II) acetate and stirred for 2 h. The resulting white precipitate of the precursor, cadmium(II)-1,2,4,5-benzenetetracarboxylate hydrate $[(C_{10}H_2O_8)Cd_2 \cdot xH_2O]$ was filtered through suction, washed several times with distilled water. The precursor complex was then divided into four portions and each portion was transferred to a porcelain crucible and calcined for 2 h in a muffle furnace. Spherical cadmium(II) oxide (CdO) nanoparticles having dimension 93, 86, 62 and 53 nm were synthesized by calcining the precursor at 450, 500, 550 and 600 °C, respectively.

3 Characterization techniques

In analytical measurements, PXRD patterns of the CdO nanoparticles were recorded with the help of Bruker D8 X-ray Diffractometer with CuK_{α} ($\lambda = 1.5418 \text{ \AA}$) radiation. The microscopic images of the CdO nanomaterials were taken by FEI, Inspect F-50 field emission scanning electron microscope (FESEM). Optical absorption spectra were recorded by Shimadzu make 2401PC spectrophotometer. The optical band gap of CdO nanoparticles were estimated with the help of Tauc's plots from UV–Vis absorption spectrum. The electrical conductivity of the materials was measured with the help of Keithley 2400 sourcemeeter. The

capacitance and other related parameters were measured using a computer controlled LCR meter (precision LCR meter Agilent E4980) as a function of frequency over a wide range of frequencies (100 Hz–2 MHz) at room temperature.

4 Results and discussions

Figure 1 represents the X-ray diffraction pattern of the synthesized materials. The responsible Bragg's planes for diffraction are (111); (200); (220); (311) and (222) at Bragg's angle $2\theta = 33.1$; 38.3; 55.3; 66.1 and 69.4, respectively, indicated that all the synthesized materials are CdO, supported by the JCPDS Card No: 65-2908 [29]. There is no change in diffraction patterns of respective Bragg's planes, only but intensity which indicated the phase identity with different crystallite size of the materials synthesized at different temperature. The size of the crystallites were determined as 93, 86, 62, and 53 nm, respectively, as revealed from the slope of the extrapolated linear part of Williamson Hall's plot, $B_r \cos\theta$ against $\sin\theta$, by considering modified P. Scherrer's equation [30]:

$$B_r \cos\theta = \frac{K\lambda}{D} + \mu \sin\theta \quad (1)$$

where, D is crystallite size, B_r is full width at half maxima (FWHM), μ is crystal strain and K is shape factor. The value of $K = 0.9$ was considered as standard.

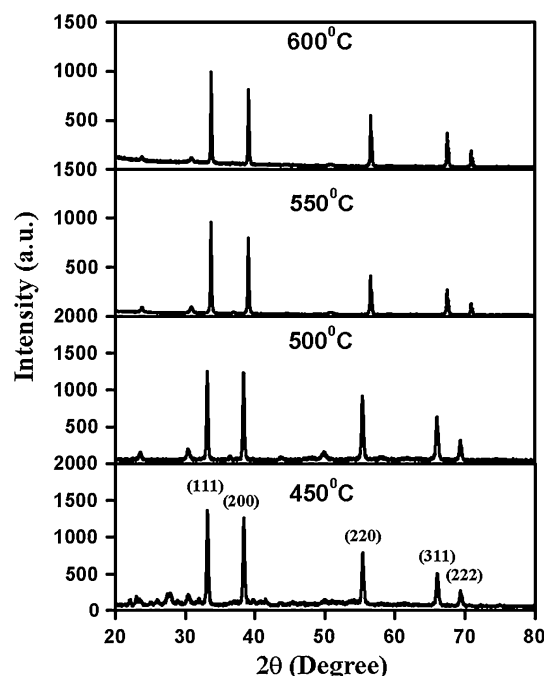


Fig. 1 Powder XRD patterns of the synthesized materials (calcination temperatures: 450, 500, 550 and 600 °C, respectively)

Figure 2a–d represents the field emission scanning electron microscopic (FESEM) images of the synthesized materials at 1 μm scale. The morphological growth of the crystallites were highly controlled by the vapour pressure and the conditional temperature. These images depict that as the conditional temperature increases during chemical growth the particle size decreases accordingly which is also supported by the estimated size of the crystallites from P. Scherrer’s method.

To investigate the morphology dependant optical behavior of the materials, UV–Vis absorption spectra of the samples in chloroform medium were recorded in the wavelength range 300–800 nm (Fig. 3). In this regards absorption coefficients for each of the samples were estimated by employing the Beer-Lamberts’ equation:

$$\alpha = \left(\frac{1}{d}\right) \ln\left(\frac{1}{T}\right) \tag{2}$$

where, *d* is the thickness of the cuvette (=10 mm) and *T* is the transmittance. To get better insight, the optical band gap energy of the nanoparticles was determined with the help of Tauc’s equation for direct optical transition [31]:

$$\alpha h\nu = A(h\nu - E_g)^{\frac{1}{2}} \tag{3}$$

where α is the optical absorption coefficient, $h\nu$ is the photon energy, E_g is the direct band gap and $A = 0.9$ is a

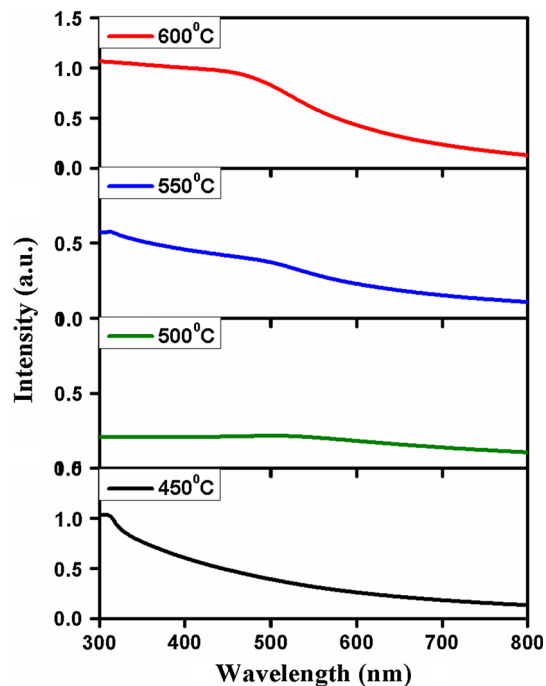


Fig. 3 UV–Vis absorption spectra of the CdOs at different conditional temperatures

constant. The direct band gap of the CdO particles were evaluated as 2.54, 2.35, 2.12 and 1.71 eV for the materials at conditional temperature 450, 500, 550 and 600 °C,

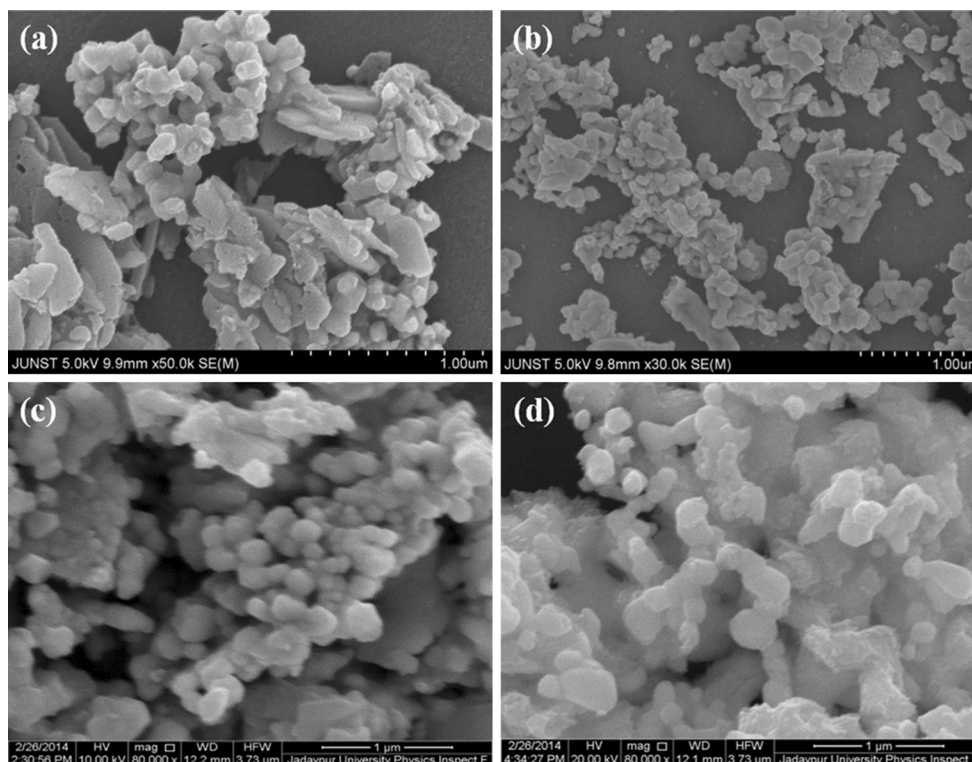


Fig. 2 SEM images of CdOs: **a** at 450 °C, **b** at 500 °C, **c** at 550 °C and **d** at 600 °C

respectively (Fig. 4) by measuring the intercept of the extrapolated linear part of the plot $(\alpha h\nu)^2$ against $(h\nu)$. The numerical order of these measured values of optical band gap signifies that the synthesized materials are belonging to the semiconductor family. The descending order of band gap energies also indicate that as the calcination temperature of the synthesis increases the rate of chemical growth of the materials is highly affected, which results in improvement of the size dependent absorption of the particles. It may be due to Burstein–Moss effect [32, 33] i.e. the shifting of absorption edge to higher energies depending upon morphology (during the nucleation of material at a certain temperature), results more population of energy states near conduction band.

To investigate light induced electrical charge transport behavior of the samples and their morphological effect on conductivity the thin film practice was adopted. The morphology dependent dark and photo conductivity of the synthesized materials were measured by recording the current–voltage characteristic (Fig. 5) at room temperature by two probe technique. In this regard we have deposited a thin film of the material on ITO coated glass substrate by

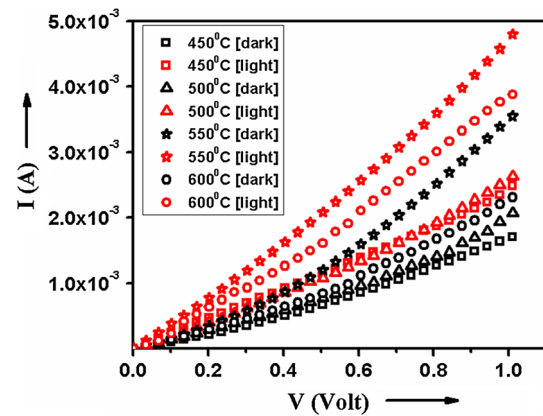


Fig. 5 Current–voltage characteristics of the samples under dark and light

spin coating technique with a constant spin rate (1600 rpm) for each sample. The films were sensitized by the radiation of white light of illumination 100 mWcm^{-2} . Photosensitivity, the measure of ratio of photo-conductivity to dark-conductivity, was estimated for each film. The measured values are enlisted in Table 1. From the data of Table 1 it

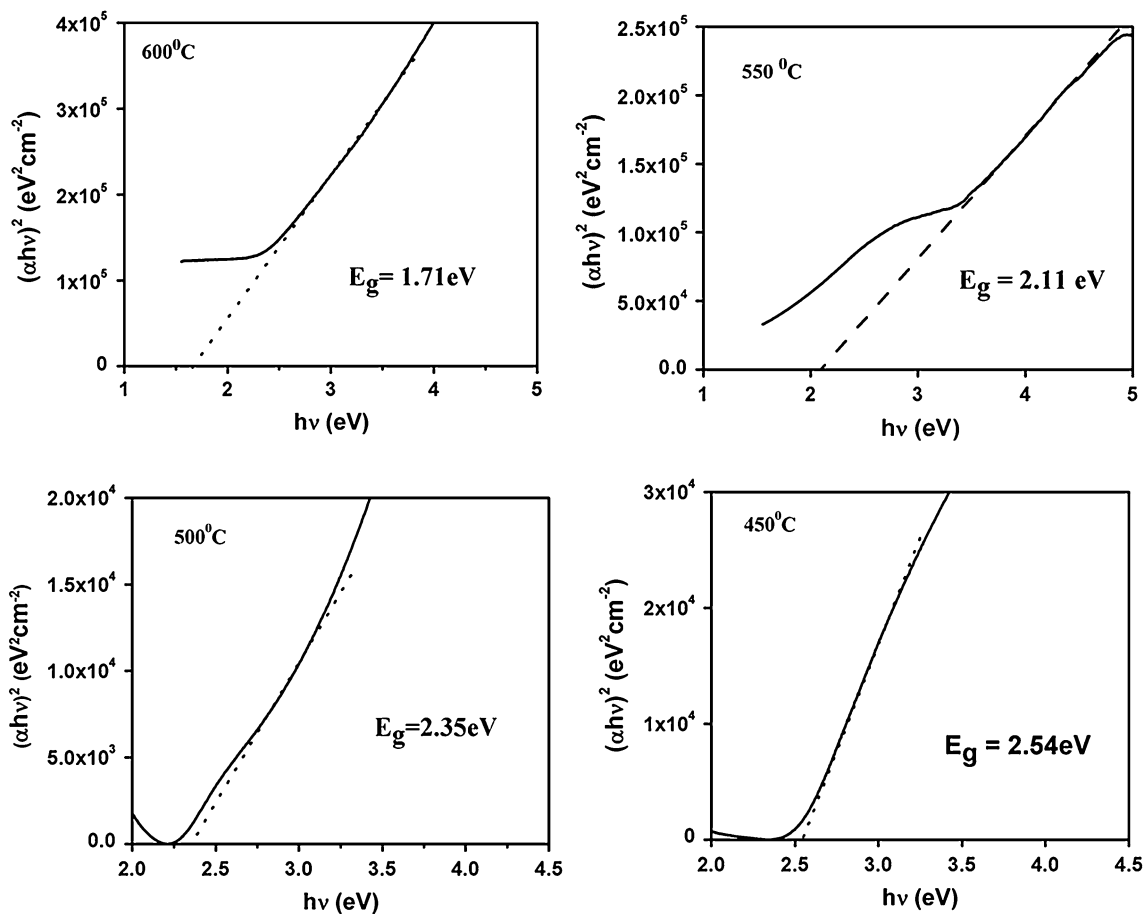


Fig. 4 Band gap energy of the materials from Tauc's plots

is very clear that after light soaking the photo induced carriers’ transport phenomena had been accelerated accordingly depending upon the dimensions of the nano crystallites as well as their effective surface area.

To get better insight of electrical charge transport phenomena one should realize the dielectric environment produced inside of materials. Thus to study the dielectric behavior of the synthesized materials four identical pallets of the CdOs were prepared in same ambient conditions and their thicknesses were measured with the help of surface profiler. The capacitance of the material pallets were recorded against applied frequency at constant voltage. Figure 6 shows capacitance versus frequency plot of the materials at room temperature. It shows that for each sample the capacitance initially falls sharply as the frequency increases and then saturates to some value as the frequency approaches 2 MHz. As revealed from Fig. 6, the ratio of low frequency to high frequency capacitance obtained are found to be close to 1.1:1, 3.8:1, 2.1:1 and 3.3:1 whereas the ratio of low frequency to high frequency impedance obtained from Fig. 7 is found to be 266:1, 225:1, 397:1, 189:1, respectively. The high capacitance and high impedance at lower frequencies may be attributed to the significant polarization of charge carriers [34, 35]. The dipoles cannot orient themselves at higher frequencies and hence the capacitance as well as impedance decreases. However, for Debye relaxation process the low frequency to high frequency capacitance ratio is expected typically to be 3:1 [36, 37] while the observed ratio in case of our materials are 1.1:1, 3.8:1, 2.1:1 and 3.3:1, respectively.

The dielectric constant was evaluated with the help of the equation:

$$\epsilon = 11.3CL/A \tag{4}$$

where C is the capacitance in pF unit, L is the length and A is the effective area of the sample pallet. Figure 8 shows the variation of dielectric constant of the sample with frequency at room temperature. The dielectric constant shows a decreasing trend for the samples. This decrease is rapid at lower frequency and slower but stable at higher frequency for the sample grown at 550 and 600 °C. The decrease of dielectric constant with increasing frequency is a normal dielectric behavior which is also observed by other researchers [38–40]. A ceramic material that can experience interfacial polarization as predicted by Maxwell

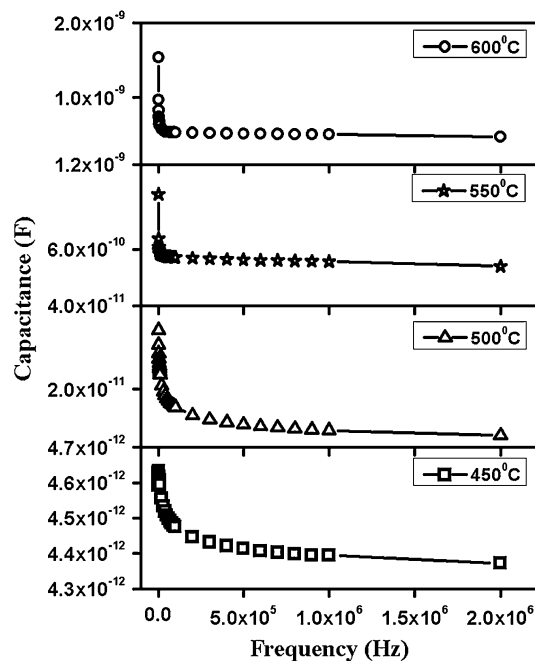


Fig. 6 Capacitance against frequency plots

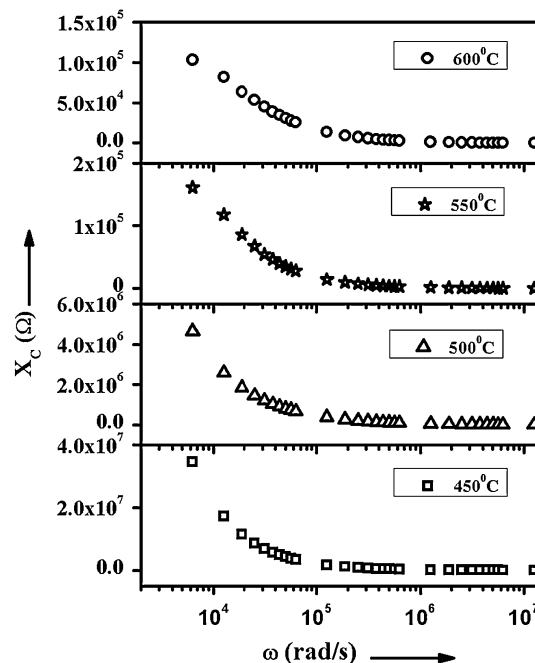


Fig. 7 Impedance verses frequency plots

Table 1 Room temperature dark and photoconductivity

Sample	Dark conductivity (S cm ⁻¹)	Photo-conductivity (S cm ⁻¹)	Photosensitivity
CdO at 450 °C	9.68 × 10 ⁻⁷	12.42 × 10 ⁻⁷	1.28
CdO at 500 °C	10.98 × 10 ⁻⁷	14.44 × 10 ⁻⁷	1.32
CdO at 550 °C	20.16 × 10 ⁻⁷	28.63 × 10 ⁻⁷	1.42
CdO at 600 °C	12.91 × 10 ⁻⁷	22.31 × 10 ⁻⁷	1.73

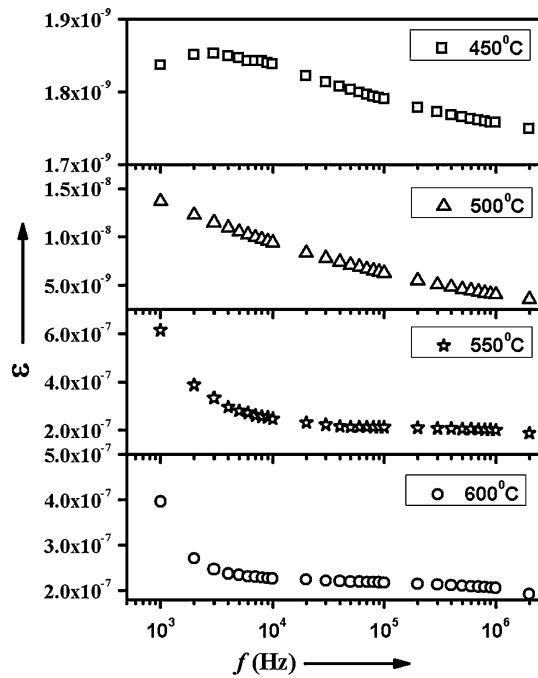


Fig. 8 Dielectric constant against frequency plots

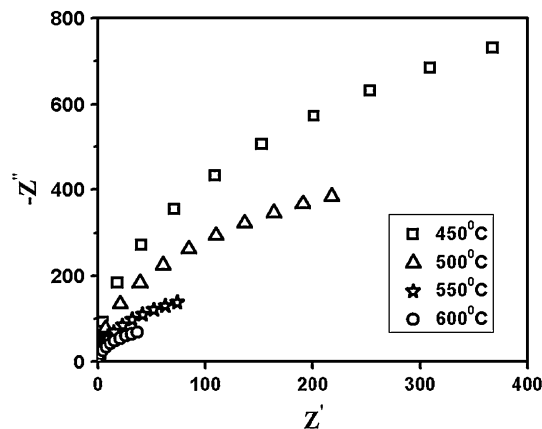


Fig. 9 Nyquist plots (complex impedance spectra)

and Wagner. They pointed out that at low frequency region the movement of charge carriers trapped at interfacial region which is caused by inhomogeneous dielectric structure. At high frequency, the dominant mechanism contributing to dielectric constant is the hopping mechanism in their respective interstice under the influence of alternating current. The frequency of hopping between ions could not follow the frequency of applied field and hence it lags behind, therefore the values of dielectric constant become reduced at higher frequency [41]. A low loss factor is desirable for a dielectric material so that the dissipated electric power to the insulator is minimized. This type of consideration is very important for high power circuits operating at high speed. Dissipation factor is a ratio of the

energy dissipated to the energy stored in the dielectric material. The more energy that is dissipated into the material, the less is going to make it to the final destination. This dissipated energy typically turns into heat or is radiated as radio frequency (RF) into the air. The optimal goal is to have 100 % of the signal pass through the interconnection network and not be absorbed in the dielectric. A high loss material means a little or no signal is left at the end of the transmission path. In order to retain maximum signal power, a low loss material should be used. The defect, space charge formation and lattice distortion is believed to produce an absorption current resulting in a loss factor and at high alternating frequency those could follow the field applied and at later values the trend saturated [41].

Moreover, to investigate the detail of effecting impedance occurring inside the sample's environment, the complex impedance spectra analysis is obligatory. Figure 9 shows complex impedance spectra (Nyquist plot) of the compounds, over a wide range of frequency (1 kHz–1 MHz). The immittance property of the materials was characterized by the appearance of semicircular arcs whose pattern of evolution was changed with change in morphology. The extent of intercept on the real axis provides very important information on electrical behavior of the material under investigation. Such pattern illustrates the kind of electrical processes occurring within the material and their correlation with microstructure when modeled in terms of an equivalent electric circuit. The extended curves produced semicircular arc of the impedance pattern can mainly be attributed to a parallel combination of resistance and capacitance. Depending upon morphology of the material the centre of progressive semicircles shifted towards origin of the complex plane plot which depicts not only that the bulk resistance of the material was decreased but also the small contribution of grain boundary within the material [41].

Figure 10 represents the variation of loss tangent ($\tan\delta$) of the samples with frequency. All these plots indicate that $\tan\delta$ decreases with increase of frequency and attains a minimum value which is generally feature of polar dielectric materials. Figure 10 illustrates that the dielectric loss which is basically a part of energy of electric field dissipated as heat, decreased rapidly in lower frequency regime and saturated at higher frequencies. This is because in lower frequency region, the carrier transport through unpolarized material is controlled by the applied field whereas in higher frequency regime the carrier transportation is governed by the field arisen due to polarized medium [37]. The most important thing is to be noted that the loss of energy varies depending upon the grain size of the particle. This might be due to occurrence of grain boundaries depending upon the morphology of the particles. The presence of a large number of grain boundaries

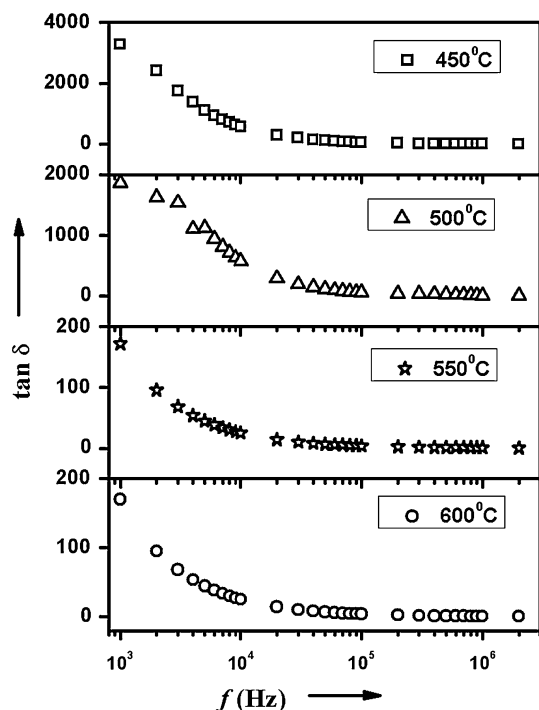


Fig. 10 Loss-tangent against frequency plots

produces localized field in grain interiors where the conduction of carrier dominated by hopping results in loss of energy. Hence in subject to transport AC signal through CdO, one has to minimize the dimension of the particle. In our case CdO, synthesized at 600 °C is more promising candidate in fabrication of signal transporting network than the others.

5 Conclusion

In this paper we have employed a cost effective chemical reduction method for the synthesis of CdO nanomaterials using a new cadmium(II)-1,2,4,5-benzenetetracarboxylate hydrate precursor. We have explored the role of triethylamine, an unconventional base, in the synthesis of these materials which also confirms its applicability in the synthesis of metal oxide nanoparticles as a substitute of the conventional hydroxide bases. The synthesized nanomaterials are primarily characterized by PXRD and FESEM analyses. It was observed that the morphology of materials strongly depend on the calcination temperature and reduction of size of the particle was observed with the increase of the temperature. The effect of morphology on the optical properties of the materials was studied which reveal that the decrease of particle size leads to lowering optical band gap and the absorption maximum undergoes bathochromic shift. The photo-sensing behavior of the material was improved depending upon the minimal size of

the grains. The morphology dependent dielectric behavior was analyzed by intervening into frequency allied complex impedance and loss-tangent. Thus it can be conclude that among these novel CdOs the compound grown at 600 °C could be a promising one in the application of signal transporting network.

Acknowledgments S. Shit gratefully acknowledges University Grants Commission, New Delhi, India for financial assistance [Minor Research Project No. F. PSW-65/12-13 (ERO)]. Authors acknowledge the Department of Physics, Jadavpur University, Kolkata, India for technical support.

References

1. T. Trindade, P. O'Brien, N.L. Pickett, Nanocrystalline semiconductors: synthesis, properties, and perspectives. *Chem. Mater.* **13**, 3843–3858 (2001)
2. A. Thiaville, J. Miltat, Small is beautiful. *Science* **284**, 1939–1940 (1999)
3. T. Aswani, B. Babu, V.P. Manjari, R.J. Stella, G.T. Rao, C.R. Krishna, R.V.S.S.N. Ravikumar, Synthesis and spectral characterizations of trivalent ions (Cr^{3+} , Fe^{3+}) doped CdO nanopowders. *Spectrochim. Acta* **121A**, 544–550 (2014)
4. K. Kaviyarasu, E. Manikandan, P. Paulraj, S.B. Mohamed, J. Kennedy, One dimensional well-aligned CdO nanocrystal by solvothermal method. *J. Alloys Comp.* **593**, 67–70 (2014)
5. A. Gulino, G. Compagnini, A. Scalisi, Large third-order nonlinear optical properties of cadmium oxide thin films. *Chem. Mater.* **15**, 3332–3336 (2003)
6. P. Gadanne, Y. Yagil, G. Deutscher, Transmittance and reflectance *in situ* measurements of semicontinuous gold film during deposition. *J. Appl. Phys.* **66**, 3019–3025 (1989)
7. P. Yang, C.M. Lieber, Nanorod-superconductor composites: a pathway to materials with high critical current densities. *Science* **273**, 1836–1840 (1996)
8. R.J. Bandaranayake, G.W. Wen, J.Y. Lin, H.X. Jiang, C.M. Sorensen, Structural phase behavior in II–VI semiconductor nanoparticles. *Appl. Phys. Lett.* **67**, 831–833 (1995)
9. F. Yakuphanoglu, M. Caglar, Y. Caglar, S. Ilican, Electrical characterization of nanocluster n-CdO/p-Si heterojunction diode. *J. Alloys Comp.* **506**, 188–193 (2010)
10. M. Aksoy, C. Aydin, F. Yakuphanoglu, I.S. Yahia, Nanopowder synthesis of aluminum doped cadmium oxide via sol-gel calcination processing. *J. Alloys. Compd.* **509**, 854–858 (2011)
11. R. Vinodkumar, K.J. Lethy, P.R. Arunkumar, R. Krishnan, N. Venugopalan Pillai, V.P. Mahadevan Pillai, Effect of cadmium oxide incorporation on the microstructural and optical properties of pulsed laser deposited nanostructured zinc oxide thin. *Mater. Chem. Phys.* **121**, 406–413 (2010)
12. A.V. Moholkar, G.L. Agawane, K.-U. Sim, Y.-B. Kwon, K.Y. Rajpure, J.H. Kim, Influence of deposition temperature on morphological, optical, electrical and opto-electrical properties of highly textured nano-crystalline spray deposited CdO: Ga thin films. *Appl. Surf. Sci.* **257**, 93–101 (2010)
13. R.K. Gupta, K. Ghosh, R. Patel, P.K. Kahol, Low temperature processed highly conducting, transparent, and wide bandgap Gd doped CdO thin films for transparent electronics. *J. Alloys Comp.* **509**, 4146–4149 (2011)
14. M.H. Kim, Y.-U. Kwon, Semiconductor CdO as a blocking layer material on DSSC electrode: mechanism and application. *J. Phys. Chem. C* **113**, 17176–17182 (2009)

15. H. Zhou, T. Fan, D. Zhang, Hydrothermal synthesis of ZnO hollow spheres using spherobacterium as biotemplates. *Microporous Mesoporous Mater.* **100**, 322–327 (2007)
16. H.B. Lu, L. Liao, H. Li, Y. Tian, D.F. Wang, J.C. Li, Q. Fu, B.P. Zhu, Y. Wu, Fabrication of CdO nanotubes via simple thermal evaporation. *Mater. Lett.* **62**, 3928–3930 (2008)
17. D.S. Dhawale, A.M. More, S.S. Latthe, K.Y. Rajpure, C.D. Lokhande, Room temperature synthesis and characterization of CdO nanowires by chemical bath deposition (CBD) method. *Appl. Surf. Sci.* **254**, 3269–3273 (2008)
18. Y.C. Zhang, G.L. Wang, Solvothermal synthesis of CdO hollow nanostructures from CdO₂ nanoparticles. *Mater. Lett.* **62**, 673–675 (2008)
19. S.H. Tolbert, A.P. Alivisatos, The Wurtzite to rock-salt structural transformation in CdSe nanocrystals under high pressure. *J. Chem. Phys.* **102**, 4642–4656 (1995)
20. N. Herron, Y. Wang, H. Eckert, Synthesis and characterization of surface-capped, size-quantized CdS clusters. Chemical control of cluster size. *J. Am. Chem. Soc.* **112**, 1322–1326 (1990)
21. G. Chiu, E.J. Meehan, The preparation of monodisperse lead sulfide sols. *J. Colloid Interface Sci.* **49**, 160–161 (1974)
22. P.P. Sharmila, R.M. Sebastain, S. Sagar, E.M. Mohammed, N.J. Tharayil, Dielectric properties and conductivity of (ZnO/CdO) mixed oxide nanocomposite. *Ferroelectrics* **474**, 144–155 (2015)
23. V. Safarifard, A. Morsali, Sonochemical syntheses of a nanoparticles cadmium(II) supramolecule as a precursor for the synthesis of cadmium(II) oxide nanoparticles. *Ultrason. Sonochem.* **19**, 1227–1233 (2012)
24. M. Ramazani, A. Morsali, Sonochemical syntheses of a new nano-plate cadmium(II) coordination polymer as a precursor for the synthesis of cadmium(II) oxide. *Ultrason. Sonochem.* **18**, 1160–1164 (2011)
25. A. Mehrani, A. Morsali, Synthesis and crystal structures of mercury(II) and cadmium(II) coordination compounds using 4'-(4-pyridyl)-2,2':6',2'-terpyridine ligand and their thermolysis to nanometal oxides. *J. Mol. Struct.* **2014**, 596–601 (1074)
26. S. Geranmayeh, A. Abbasi, Simultaneous growing of two new Cd(II) metal-organic frameworks with 2,6-Naphthalendicarboxylic acid as new precursors for cadmium(II) oxide nanoparticles: thermal, topology and structural studies. *J. Inorg. Organomet. Polym.* **23**, 1138–1144 (2013)
27. M. Payehghadr, V. Safarifard, M. Ramazani, A. Morsali, Preparation of cadmium(II) oxide nanoparticles from a new one-dimensional cadmium(II) coordination polymer precursor; spectroscopic and thermal analysis studies. *J. Inorg. Organomet. Polym.* **22**, 543–548 (2012)
28. S. Shit, T. Kamilya, P.K. Samanta, A novel chemical reduction method of growing ZnO nanocrystals and their optical property. *Mater. Lett.* **114**, 123–125 (2014)
29. D.M. Yufanyi, J.F. Tendo, A.M. Ondoh, J.K. Mbadcam, CdO nanoparticles by thermal decomposition of a Cd-hexamethylenetetramine complex. *J. Mater. Sci. Res.* **3**, 1–11 (2014)
30. A. Monshi, Modified Scherrer equation to estimate more accurately nano-crystallite size using XRD. *World J. Nano Sci. Eng.* **2**, 154–160 (2012)
31. J. Tauc, A. Menth, States in the gap. *J. Non-Cryst. Solids* **8–10**, 569–585 (1972)
32. Y. Abdollahi, A.H. Abdullah, Z. Zainal, N.A. Yusof, Synthesis and characterization of manganese doped ZnO nanoparticle. *Int. J. Basic Appl. Sci.* **11**, 44–50 (2011)
33. P. Chakraborty, G. Datta, K. Ghatak, A simple theoretical analysis of the effective electron mass in heavily doped III–V semiconductors in the presence of band-tails. *Phys. Scr.* **68**, 368–377 (2003)
34. J.C. Maxwell, *Electricity and Magnetism* (Oxford University Press, London, 1973)
35. K.W. Wagner, Dissipation of energy under AC. *Ann. Phys.* **40**, 817–855 (1913)
36. O.S. Panwar, M. Radhakrishana, K.K. Srivastava, Electrical and dielectric properties of As₁₀Ge₁₅Te₇₅Ag_x glasses. *Philos. Mag. B* **41**, 253–271 (1980)
37. A. Layek, A. Dey, J. Datta, M. Das, P.P. Ray, Novel CuFeS₂ pellet behaves like a portable signal transporting network: studies of immittance. *RSC Adv.* **5**, 34682–34689 (2015)
38. H.M. Chenari, A. Hassanzadeh, M.M. Golzan, H. Sedghi, M. Talebian, Frequency dependence of ultrahigh dielectric constant of novel synthesized SnO₂ nanoparticles thick films. *Curr. Appl. Phys.* **11**, 409–413 (2011)
39. B.H. Venkataraman, K.B.R. Varma, Frequency-dependent dielectric characteristics of ferroelectric SrBi₂Nb₂O₉ ceramics. *Solid State Ion.* **167**, 197–202 (2004)
40. D. Ravinder, G. Ranga Mohan, N. Prankishan, D.R. Sagar, High frequency dielectric behaviour of aluminium-substituted lithium ferrites. *Mater. Lett.* **44**, 256–260 (2000)
41. G.B. Kumar, S. Buddhudu, Optical, thermal and dielectric properties of Bi₄(TiO₄)₃ ceramic powders. *Ceram. Int.* **36**, 1857–1861 (2010)